PCCP
Physical Chemistry Chemical Physics

Accepted Manuscript

This article can be cited before page numbers have been issued, to do this please use: M. Nagasaka, S. Okumura, S. Ichii, G. Hamasaka and Y. Uozumi, *Phys. Chem. Chem. Phys.*, 2026, DOI: 10.1039/D6CP00617E.

View Article Online
DOI: 10.1039/D6CP00617E

ARTICLE

Using soft X-ray absorption spectroscopy to evaluate the electronic structures of sp^2-hybridized carbons in organic solvents

Masanari Nagasaka,*[a] Shintaro Okumura,*[ab] Shun Ichii,[a] Go Hamasaka,[a] and Yasuhiro Uozumi*[a]

Received 00th January 20xx,
Accepted 00th January 20xx

DOI: 10.1039/x0xx00000x

The reactivity of an organic compound is often discussed in relation to the bond length at the reaction site. However, obtaining such information in organic solvents, where most organic reactions occur, remains a demanding task. Here, we analyze the electronic structures of organic molecules containing sp^2 carbons in organic solvents using soft X-ray absorption spectroscopy (Soft-XAS-OS). By determining the energy thresholds of representative organic solvents, we confirmed that the electronic states of sp^2 carbons can be distinguished from solvent absorption. Soft-XAS-OS was applied to study the Hiyama cross-coupling reaction. The observed XAS spectra of arylsilanes in organic solvents were rationalized in terms of C–Si bond elongation through the inner-shell calculations combined with molecular dynamics simulations. The reactive glycol-derived silicate Ph–Si$(OCH_2CH_2O)_2$ exhibited longer C–Si bonds in solution than the less reactive Ph–Si$(OMe)_3$. These findings demonstrate that Soft-XAS-OS, combined with inner-shell calculations, provides a powerful method for probing electronic structures and gaining insights into the bond lengths related to sp^2 carbons in organic solvents.

1. Introduction

Bond lengths in organic compounds are among the key factors that determine their reactivity. For example, the structure-correlation principle was initially developed by Dunitz and Kirby.[1-8] Jones and Kirby reported that, in the hydrolysis of acetals, there is a linear correlation between the bond length at the reaction site and the activation free energy of its cleavage.[6] However, such discussions have previously been limited to comparing the reactivity of an organic compound in solution with its bond length in the solid state, given that the covalent bond length is usually measured using X-ray diffraction (XRD) techniques. XRD requires a single-crystal sample with a three-dimensional periodic arrangement; thus samples in solutions with a non-uniform arrangement are not suitable for XRD studies (Fig. 1(a)). Therefore, obtaining information on the length of a reactive bond in organic solvents, where most organic reactions take place, is a demanding task for understanding its reactivity. Although nuclear magnetic resonance (NMR), UV-visible (UV-vis), and infrared (IR) spectroscopic measurements provide valuable insights into chemical structures in solution, these techniques are generally unsuitable for evaluating bond lengths.

X-ray absorption spectroscopy (XAS) is one type of molecular spectroscopy that measures the X-ray transmission of samples in the gas, liquid, and solid phases. The XAS peaks correspond to the transitions of the core electrons to unoccupied orbitals. The electronic structure of different elements can be measured separately using different absorption edges. Information relating to different functional groups constructed from the same elements can also be obtained owing to the energy differences of the unoccupied orbitals. The energy shifts of the XAS peaks also reflect differences in molecular interactions, such as hydrogen bonds and dipole interactions.[9] The electronic structures of organic molecules can be connected to the bond lengths of organic molecules and molecular interactions of solvent molecules using the inner-shell calculations. The K-edges of transition metals are located in the hard X-ray regions. Accordingly, the bond lengths and coordination numbers between central metals and ligands in metal complexes have been investigated using the extended X-ray absorption fine structure, leading to a better understanding of the catalytic activity of transition metals.[10,11]

However, organic molecules mainly consist of light elements (*e.g.*, C, N, O, and F), and the reactivity and bond length of organic molecules should be investigated using XAS in the soft X-ray region (< 1 keV), which includes K-edges of light elements. Because soft X-rays are strongly absorbed by air and liquids,[12] the XAS measurements mainly applied to solid samples under vacuum or atmospheric helium condition and are difficult to apply liquid samples. Several new detection techniques enable the application of the XAS measurements to liquid samples.[13] To obtain the XAS spectra of liquid samples in transmission mode, the liquid layer in the liquid cell is sandwiched between two Si_3N_4 membranes (thickness: 100 nm), and the thickness of the liquid layer can be precisely controlled in a range from 20 nm to 40 μm by adjusting the helium pressure around the liquid cell.[14, 15] As shown in Fig. 1(b), in aqueous solution, the C and N

[a] Institute for Molecular Science, Myodaiji, Okazaki 444-8787, Japan. E-mail: nagasaka@ims.ac.jp, uo@ims.ac.jp
[b] Department of Synthetic Chemistry and Biological Chemistry, Kyoto University, Kyoto 615-8510, Japan. E-mail: okumura.shintaro.6e@kyoto-u.ac.jp

† Electronic Supplementary Information (ESI) available. See DOI: 10.1039/x0xx00000x

View Article Online
DOI: 10.1039/D6CP00617F

K-edge XAS spectra of organic molecules can be measured using the water-window technique,[16-18] where the K-edges of C (~280 eV) and N (~400 eV) show high transmission of soft X-rays in aqueous solution since these energy regions are below the O K-edge (~530 eV). The local structures of methanol,[19] ethanol,[20] 1-butanol,[21] pyridine,[22] pyridazine,[23] and acetonitrile[24] in aqueous solution have been investigated using C and N K-edge XAS (Soft-XAS-H_2O). However, the majority of organic reactions are conducted in organic solvents, and the C and N K-edge XAS absorbances of organic molecules are expected to overlap with those of the organic solvent.

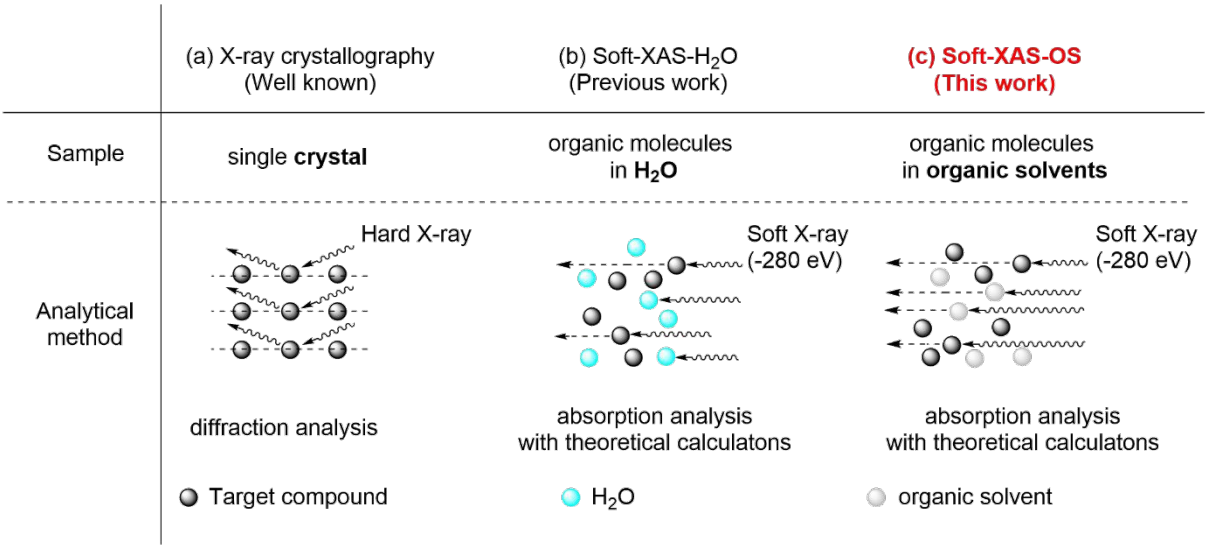

Fig. 1 Measurements for obtaining bond-length information of sp^2-hybridized carbon atoms. (a) X-ray crystallography of organic molecules in single crystals. (b) C K-edge XAS of organic molecules in H_2O (Soft-XAS-H_2O). (c) C K-edge XAS of organic molecules in organic solvents (Soft-XAS-OS).

The C K-edge XAS spectrum of cyanopyrazine in ethanol–water binary solution exhibits the C=C π* (285.4 eV) and C=N π* peaks (286.0 eV) located below the absorption of ethanol (286.5 eV).[25] Accordingly, the electronic structures of the sp^2-hybridized C=C and C=N π orbitals of organic molecules can be observed, distinct from the strong absorbances of the sp^3-hybridized C–C and C–O orbitals of organic solvent molecules. Building on this finding, we establish here a new C K-edge XAS technique, termed 'Soft-XAS-OS', to analyze the electronic structures of organic molecules that contain sp^2-hybridized carbons in organic solvents (Fig. 1(c)). To assess its feasibility, we measured the energy thresholds of representative organic solvents and the energies of various sp^2-hybridized carbons. Then, Soft-XAS-OS was applied to investigate the electronic structures of arylsilanes and silicates, which exhibit different reactivity in the Hiyama cross-coupling reaction, a reaction that we have previously examined.[26] Through comparison with inner-shell calculations combined with molecular dynamics (MD) simulations, Soft-XAS-OS provides insights into the reactive bond lengths in organic solvents.

2. Results and discussion

2.1. C K-edge Soft-XAS-OS experiments of common organic solvents and various sp^2-hybridized carbon atoms

Figure 2 shows the C K-edge XAS spectrum of 100 mM Ph–$Si(OMe)_3$ in THF. The XAS spectra were measured using a transmission-type liquid cell[14, 15] at the soft X-ray beamline BL3U of the UVSOR-III Synchrotron.[27] The strong absorbance of the THF solvent was observed at > 286.0 eV. The C=C π* peaks of Ph–$Si(OMe)_3$ appeared at ~285 eV. Although the amount of Ph–$Si(OMe)_3$ present is extremely small compared to the amount of THF, the C=C π* peaks of Ph–$Si(OMe)_3$ can be observed clearly. It is because the energetic position of sp^2-hybridized carbons in Ph–$Si(OMe)_3$ is lower than the energy threshold (pre-edge feature) of THF. To evaluate the feasibility of Soft-XAS-OS, we examined the energy thresholds of representative organic solvents and energetic positions of the π* peaks in organic molecules that contain sp^2-hybridized carbons.

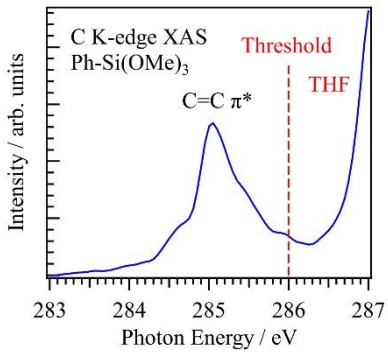

Fig. 2 C K-edge XAS spectrum of 100 mM Ph–$Si(OMe)_3$ in THF. The energy threshold of THF is shown in a dashed line.

Table 1 shows the energy thresholds of representative organic solvents obtained from their C K-edge XAS spectra (for details, see Sec. 2 of ESI). Hexane contains only sp^3-hybridized

View Article Online
DOI: 10.1039/D6CP00617F

carbons, and its energy threshold is 286.2 eV. The energy thresholds of THF, methanol, ethanol, and ethylene glycol (EG), all molecules that bear ether and alcohol groups, are 286.0, 287.6, 286.5, and 287.8 eV, respectively. The energy threshold of dimethyl sulfoxide, which contains sulfonyl groups, is 286.2 eV. Although carbonyl groups contain sp^2-hybridized carbon atoms, the C=O π* peaks appear at high energies.[28] Thus, acetic acid (287.0 eV), *N*,*N*-dimethylformamide (287.2 eV), and acetone (286.2 eV) can be used as organic solvents for the XAS analysis of sp^2-hybridized carbons. Although acetonitrile includes a cyano group, its energy threshold is 286.4 eV.

Table 2 shows the energies of the C=C and C=N π* peaks of organic molecules containing sp^2-hybridized carbon atoms as obtained from C K-edge XAS spectra (for details, see Sec. 3 of ESI). The C=C π* peaks of aromatic compounds such as benzene, toluene, and chlorobenzene are 285.1, 285.2, and 285.2 eV, respectively. The *ortho* carbons of pyridine give rise to C=N π* peaks (285.5 eV), while the *meta* and *para* carbons result in C=C π* peaks (285.0 eV). These results suggest that the C=C and C=N π* peaks of arenes can be analyzed in organic solvents by XAS. The C=C π* peak of 1-hexene, an aliphatic olefin, is 285.0 eV, and that of 2,3-dimethyl-2-butene, a tetrasubstituted olefin, is 285.4 eV, indicating that the C=C π* peaks of olefins also can be measured in organic solvents. The C=C π* peak of ethyl acrylate is 284.5 eV.

Table 1 Energy thresholds (pre-edge features) of organic solvents at the C K-edge.

Organic solvent	Threshold / eV
Hexane	286.2
Tetrahydrofuran (THF)	286.0
Methanol[19]	287.6
Ethanol[20]	286.5
Ethylene glycol (EG)	287.8
Dimethyl sulfoxide	286.2
Acetic acid	287.0
N,*N*-Dimethylformamide	287.2
Acetone	286.2
Acetonitrile[24]	286.4

Table 2 The energies of the C=C π* peaks at the C K-edge of organic molecules that contain sp^2-hybridized carbon atoms (it should be noted here that the *ortho* carbons of pyridine relate to C=N π* peaks; all energies are given to one decimal place).

Organic molecule	Site	Energy / eV
Benzene[29]		285.1
Toluene		285.2
Chlorobenzene		285.2
Pyridine[22]	*ortho*	285.5
	meta and *para*	285.0
1-Hexene		285.0
2,3-Dimethyl-2-butene		285.4
Ethyl acrylate		284.5

2.2. The Hiyama cross-coupling reaction

The cross-coupling reaction of arylsilanes with aryl halides, the so-called Hiyama cross-coupling reaction, has emerged as a valuable method for the formation of C–C bonds, owing to its low toxicity, low cost, and the wide availability of organosilanes. However, C–Si bonds generally exhibit low reactivity, and thus, high loadings of a palladium catalyst are often required, which leads to serious problems related to the contamination of the resulting products by toxic palladium metal.[30, 31] In this context, the development of a version of the Hiyama cross-coupling reaction that uses lower palladium loadings would be highly desirable.

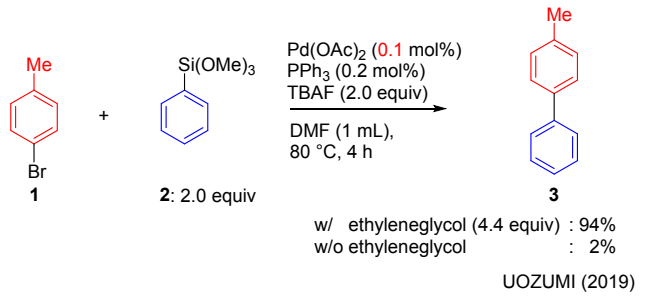

Scheme 1 Hiyama cross-coupling reaction of aryltrimethoxysilanes activated by ethylene glycol.

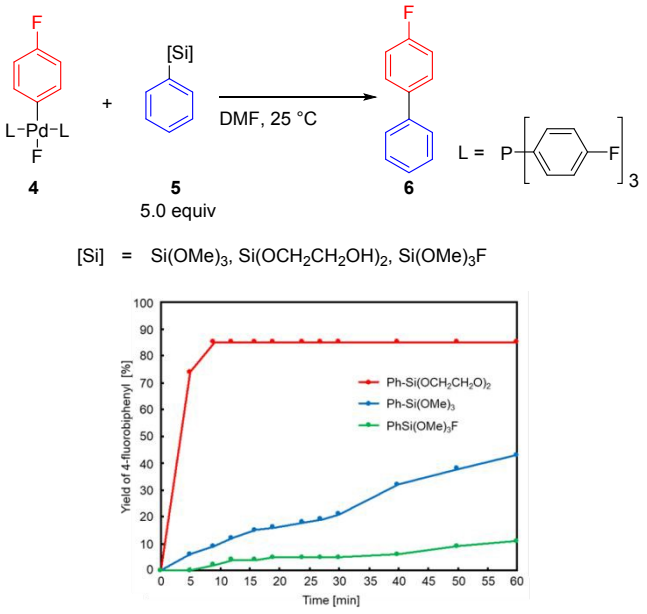

Scheme 2 Stoichiometric reactions of an arylpalladium fluoride with organosilanes.

We previously revealed that ethylene glycol promoted the Hiyama cross-coupling reactions of 4-bromotoluene (**1**) with Ph–Si(OMe)$_3$ (**2**) to give biaryl **3** (Scheme 1). In the presence of ethylene glycol, the reaction proceeded with one tenth of the amount of palladium catalyst, i.e., significantly less than the amount required in the absence of ethylene glycol.[26] After screening the reaction conditions, just 5 mol ppm of the palladium catalyst was sufficient to afford 4-fluorobiphenyl (**3**) in >99% yield.[26] The rate-determining step of the Hiyama cross-coupling is known to be the transmetallation between Ar–Si(OMe)$_3$ and the Ar'–[Pd]–F species that is generated through the oxidative addition of Ar'–X onto palladium, followed by ligand exchange with fluoride.[32] Consistent with this

View Article Online DOI: 10.1039/D5CP00175E

mechanism, the glycol-derived spirosilicate Ph–Si(OCH_2CH_2O)$_2$ exhibited higher reactivity than Ph–Si(OMe)$_3$ and fluorosilicate Ph–Si(OMe)$_3F^-$ in stoichiometric reactions with palladium fluoride **4** (Scheme 2; for details, see Sec. 5 of ESI).

Solid-state XRD analysis showed that the C–Si bond of Ph–Si(OCH_2CH_2O)$_2$ is longer than that of Ph–Si(OMe)$_3$, supporting its higher reactivity.[26] However, the C–Si bond lengths of arylsilanes and silicates in organic solvents remain unexplored. Herein, we applied Soft-XAS-OS, in combination with inner-shell calculations, to elucidate their electronic structures and gain insights into their C–Si bond lengths in organic solvents.

2.3. Preparation of the arylsilanes

Trimethoxyphenylsilane (Ph–Si(OMe)$_3$), fluorotrimethoxyphenylsilicate (Ph–Si(OMe)$_3$F), and the ethylene-glycol-derived spirosilicate Ph–Si(OCH_2CH_2O)$_2$ were prepared (for details, see Sec. 4 of ESI).[26] Ph–Si(OMe)$_3$F was synthesized by mixing Ph–Si(OMe)$_3$ with tetrabutylammonium fluoride (TBAF, 1.0 equiv).[33] The ^{19}F NMR in THF-d_8 showed that the TBAF peak at −116.7 ppm effectively disappeared and that new peaks (−113.5, −121.0, −127.6, −136.0 ppm) emerged in the five-coordinated silicate region, indicating the formation of Ph–Si(OMe)$_3$F species with different geometries (Fig. 3D). The spectroscopic data obtained here is consistent with a report by Shukla and DeShong.[33] To assign these peaks, four possible geometries of Ph–Si(OMe)$_3$F (F-silicate 1–4) were optimized using DFT at the M062X/6-31G(d) level with the SMD solvation model (THF), and the ^{19}F NMR chemical shifts were calculated by the gauge-including atomic orbital (GIAO) method (Fig. 3A-C; for details, see Sec. 6 of ESI).[34] Accordingly, the broad peak observed at −113.5 ppm (Fig. 3D) was assigned to F-silicate 3 ($\delta_{calc.}$ = −107.41 ppm) and F-silicate 4 ($\delta_{calc.}$ = −108.02 ppm). The peaks at −121.0 ppm and −127.6 ppm are F-silicate 2 ($\delta_{calc.}$ = −119.55 ppm) and F-silicate 1 ($\delta_{calc.}$ = −125.38 ppm), respectively, indicating that F-silicate 2 is the main component of the mixture.[35]

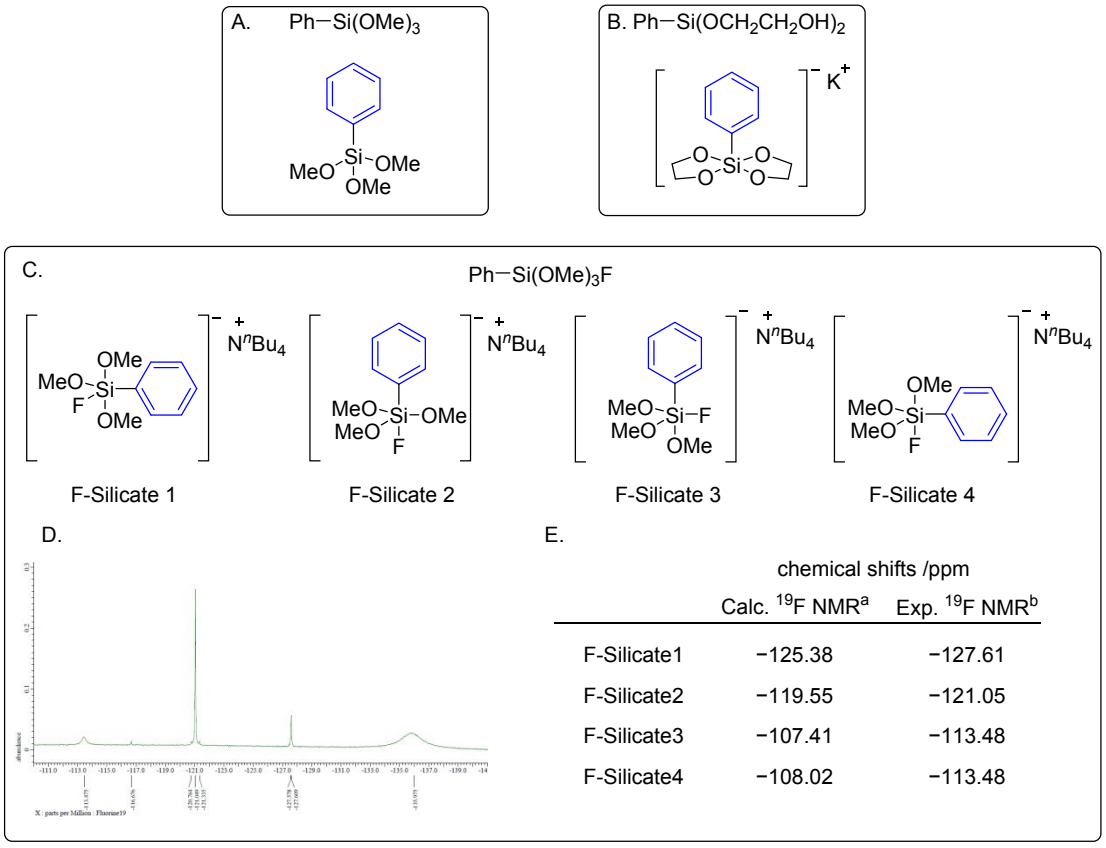

	chemical shifts /ppm	
	Calc. ^{19}F NMR[a]	Exp. ^{19}F NMR[b]
F-Silicate1	−125.38	−127.61
F-Silicate2	−119.55	−121.05
F-Silicate3	−107.41	−113.48
F-Silicate4	−108.02	−113.48

Fig. 3 The structures of (A) Ph–Si(OMe)$_3$, (B) Ph–Si(OCH_2CH_2O)$_2$, and (C) Ph–Si(OMe)$_3$F. (D) ^{19}F NMR spectrum of Ph–Si(OMe)$_3$F. (E) Comparison of the calculated and experimentally obtained chemical shifts in the ^{19}F NMR spectrum of Ph–Si(OMe)$_3$F. Geometries were optimized at the M062X/6-31G(d) level with the SMD solvation model (THF) [a] NMR data were calculated at the (GIAO) M062X/6-31G(d) level with the SMD solvation model (THF). [b] ^{19}F NMR spectrum in THF-d_8. Trifluromethylbenzene was used as the internal standard.

2.4. C K-edge XAS analysis of the arylsilanes

Soft-XAS-OS measurements were conducted for Ph–Si(OMe)$_3$, Ph–Si(OCH_2CH_2O)$_2$, and Ph–Si(OMe)$_3$F to investigate their electronic structures. As shown in Fig. 4, the C=C π* peaks of Ph–Si(OMe)$_3$ can be divided into three components, i.e., peaks A, B, and C. Peaks A, B, and C can be assigned to the *ipso*, *ortho + para*, and *meta + para* carbons of the phenyl group (*vide infra*). Thus, the C K-edge XAS can distinguish between sp^2-hybridized carbon atoms that bear different functional groups.[22] The C K-edge XAS spectra of 100 mM Ph–Si(OCH_2CH_2O)$_2$ in EG and 100 mM Ph–Si(OMe)$_3$F in THF are also shown in Fig. 4. The energetic positions of peaks A, B, and C in the arylsilane and the silicates are described in Table 3. Note that the energy shifts of the XAS peaks reflecting molecular

Journal Name ARTICLE

View Article Online
DOI: 10.1039/D6CP00617F

interactions are relatively small within 0.1 eV. The changes of hydrogen bonds in liquid water show the energy shifts within 0.1 eV in the O K-edge XAS spectra.[13, 36] The molecular interactions of pyridine[22] and acetonitrile[24] with solvent water in aqueous solutions cause the energy shifts of the XAS peaks within 0.1 eV. These peak shifts were precisely calibrated by measuring the energetic positions of the polymer films before and after the sample measurements.[37] The A peaks of the silicates appear at lower energies than that of Ph–Si(OMe)$_3$ (284.56 eV); the A peaks of Ph–Si(OCH$_2$CH$_2$O)$_2$ and Ph–Si(OMe)$_3$F are 284.54 and 284.50 eV, respectively. The B peaks of Ph–Si(OCH$_2$CH$_2$O)$_2$ (285.10 eV) and Ph–Si(OMe)$_3$F (285.09 eV) appear at higher energies than that of Ph-Si(OMe)$_3$ (285.06 eV). Note that the photon energies were calibrated by measuring XAS of the polymer film before and after the sample measurements.[37] The energy shifts within 10 meV can be evaluated owing to the energy calibration, and the errors of the photon energies were included in the results of the fitting analyses, as shown in Table 3.

Table 3 The energies of peaks A, B, and C obtained from the C K-edge XAS spectra of various silicates. The energy shifts (ΔE) relative to Ph–Si(OMe)$_3$ are also shown (all energies are given in eV).

	Peak A	ΔE	Peak B	ΔE	Peak C	ΔE
Ph–Si(OMe)$_3$	284.56 ± 0.02		285.06 ± 0.02		285.52 ± 0.04	
Ph–Si(OCH$_2$CH$_2$O)$_2$	284.54 ± 0.02	−0.02	285.10 ± 0.02	0.04	285.54 ± 0.05	0.02
Ph–Si(OMe)$_3$F	284.50 ± 0.03	−0.06	285.09 ± 0.02	0.03	285.52 ± 0.07	0.00

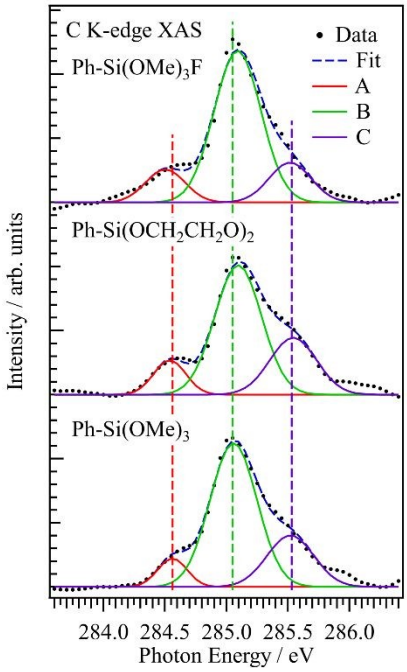

Fig. 4 C K-edge XAS spectra of 100 mM Ph–Si(OMe)$_3$, Ph–Si(OCH$_2$CH$_2$O)$_2$, and Ph–Si(OMe)$_3$F in organic solvents (Soft-XAS-OS). The dashed lines show the energies of the C=C π* peaks in Ph–Si(OMe)$_3$ obtained using a fitting procedure.

2.5. Inner-shell calculations of the arylsilanes

To understand the differences in the energies of the peaks observed in the XAS spectra of the arylsilane and the silicates, C K-edge inner-shell calculations were performed from the snapshots of the molecular dynamics (MD) simulations. The energy shifts of the XAS peaks reflect the electronic structural changes of target molecules and the molecular interactions with surrounding molecules.[15] Therefore, the changes of the C–Si bond lengths in the arylsilane and the silicates can be evaluated from the energy shifts in the inner-shell spectra of different molecular structures. The MD simulations of one arylsilane molecule with 1000 solvent molecules and several Na^+ ions for charge neutralization were performed with the 10 ns production run using the program package GROMACS 2022.4.[38] It is well known that the bond lengths of molecules are influenced by the interactions of solvent molecules.[39] The potentials of molecules were described by the OPLS-AA force field, generating using the LigParGen server.[40-42] The molecular structures of arylsilane with THF solvents were extracted from the snapshots of the MD simulations, where the distance between Si atoms and O atoms of THF or Na^+ ions were within 6.5 Å, as shown in Fig. 5. Note that the extracted molecular structures of Ph–Si(OCH$_2$CH$_2$O)$_2$ included EG solvents within the distance of 6.5 Å between Si atoms and C atoms of EG or Na^+ ions. The inner-shell spectra of the extracted molecular structures were computed by performing ΔSCF (self-consistent field) calculations of the ground and core excited states at the Hartree-Fock level using the program package GSCF3.[43, 44] Compared to the inner-shell calculations using time-dependent density functional theory, the ΔSCF method has a difficulty to reproduce the higher unoccupied orbitals but is a superior to evaluate the molecular interactions with solvent molecules owing to the SCF calculation of the excited states.[45] Because the extracted molecular structures have structural deviations,[46] the C K-edge inner-shell spectra of arylsilanes in organic solvents were obtained by averaging 1100 inner-shell spectra of the extracted molecular structures during the 10 ns production run of the MD simulations. The calculation details were provided in Sec. 7 of ESI.

Figure 5 shows the inner-shell spectrum of Ph–Si(OMe)$_3$ in THF, where the *ipso* C=C π* peak appears at 284.560 eV, while those of the *ortho*, *meta*, and *para* carbons are 285.344, 285.449, and 285.368 eV, respectively, as shown in Table 4. These results are consistent with the assignments of peaks A, B, and C in the XAS spectra of the arylsilane and the silicates (Fig. 4). Peak A is derived from the *ipso* carbon, peak B mainly from the *ortho* carbons with minor contributions from the *para* carbon, and peak C mainly from the *meta* carbons. The overall

View Article Online
DOI: 10.1039/D6CP00617F

shapes of the inner-shell spectra correspond well with those of the C K-edge XAS spectra.

In the inner-shell spectrum of Ph–Si(OCH_2CH_2O)$_2$ in EG, the C=C π* peaks are shifted relative to those of Ph–Si(OMe)$_3$ by −0.112 eV (*ipso*), −0.034 eV (*ortho*), −0.013 eV (*meta*), and 0.021 eV (*para*). In the XAS spectra shown in Fig. 4, peak A shows a lower energy shift (−0.02 eV), consistent with the energy change at the *ipso* carbon. Peak B shows a higher energy shift, reflecting the energy change at the *para* carbon. The experimental peak shifts can be rationalized in terms of energy changes of the C=C π* peaks at each carbon. Note that the inner-shell spectrum of Ph–Si(OCH_2CH_2O)$_2$ in THF also shows the same tendency that the *ipso* carbon shows a lower energy shift whereas the *para* carbon show higher energy shifts, as described in Sec. 7 of ESI.

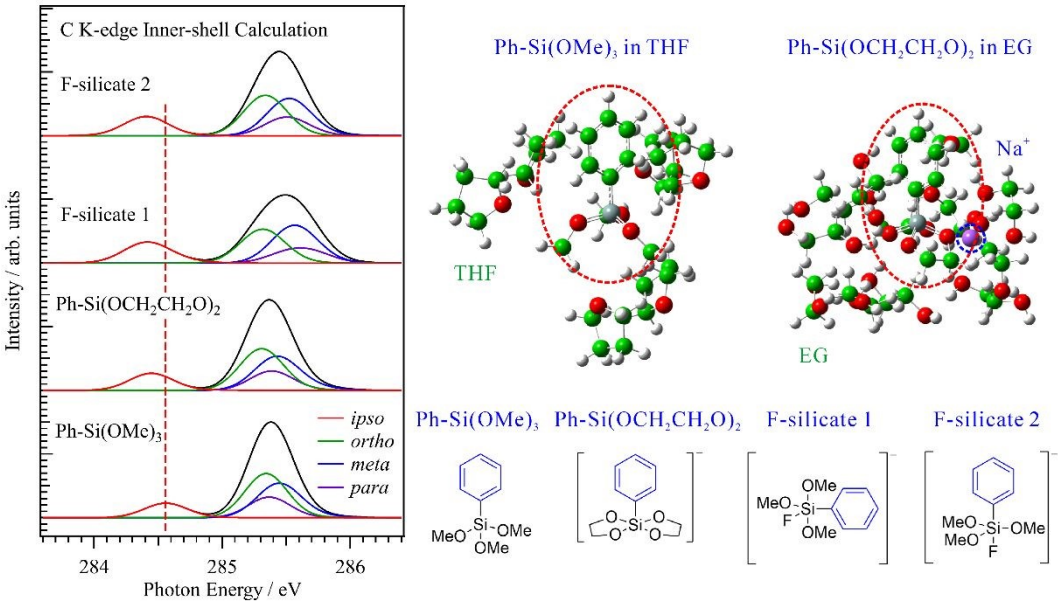

Fig. 5 Calculated C K-edge inner-shell spectra of Ph–Si(OMe)$_3$, F-silicate 1, and F-silicate 2 in THF and Ph–Si(OCH_2CH_2O)$_2$ in EG, obtained by the snapshots from the MD simulations. The snapshots of Ph–Si(OMe)$_3$ in THF and Si(OCH_2CH_2O)$_2$ in EG are shown in the inset. The energies of the *ipso*, *ortho*, *meta*, and *para* carbons in the phenyl groups were obtained. The photon energy was calibrated using the energy of the *ipso* carbons in Ph–Si(OMe)$_3$ obtained using C K-edge XAS as indicated by the dashed line.

Table 4 The energies of the *ipso*, *ortho*, *meta*, and *para* carbons obtained from C K-edge inner-shell calculations of arylsilanes. The energy shifts (Δ*E*) relative to Ph–Si(OMe)$_3$ are also shown (all energies are given in eV).

	Ipso	Δ*E*	*Ortho*	Δ*E*	*Meta*	Δ*E*	*Para*	Δ*E*
Ph–Si(OMe)$_3$	284.560		285.344		285.449		285.368	
Ph–Si(OCH_2CH_2O)$_2$	284.448	−0.112	285.310	−0.034	285.436	−0.013	285.389	0.021
F-silicate 1	284.424	−0.136	285.318	−0.026	285.570	0.121	285.608	0.240
F-silicate 2	284.406	−0.154	285.338	−0.006	285.526	0.077	285.508	0.140

The inner-shell spectrum of F-silicate 1 in THF shows a lower energy shift of the *ipso* carbon (−0.136 eV) and higher energy shifts of the *meta* (0.121 eV) and *para* carbons (0.240 eV), which are relatively close to those of Ph–Si(OCH_2CH_2O)$_2$ in EG. In contrast, F-silicate 2 shows greater shifts than Ph–Si(OCH_2CH_2O)$_2$: the *ipso* carbon of F-silicate 2 appears at lower energy by −0.154 eV relative to Ph–Si(OMe)$_3$. The *meta* and *para* carbons of F-silicate 2 are shifted to higher energies by 0.077 and 0.140 eV, respectively. These shifts explain the characteristic features of the XAS spectra of Ph–Si(OMe)$_3$F. The inner-shell calculations of other minor F-silicate derivatives such as F-silicate 3 and F-silicate 4 were listed in Sec. 7 of ESI.

These differences in C=C π* peaks can be interpreted in terms of the C(sp^2)–Si bond length. In the optimized molecular structures, the C–Si bond lengths follow the order: Ph–Si(OMe)$_3$ << Ph–Si(OCH_2CH_2O)$_2$ ≤ F-silicate 1 < F-silicate 2. The *ipso* carbons are the most strongly affected and shift to lower energies as the C–Si bond length increases. The inner-shell spectra of silicates are not influenced by solvent molecules with neutral charges such as THF, as described in Sec. 7 of ESI. The Na^+ ions affect the inner-shell spectra because the charge neutralization is necessary for silicates in organic solvents. When the charge neutralization effect is included, the energetic positions of the ipso carbons reflect the C(sp^2)–Si bond length even if there are no solvent molecules with neutral charges.

Trough comparison with inner-shell calculations, the experimental XAS spectra suggested that the C–Si bond lengths in organic solvents also followed the order: Ph–Si(OMe)$_3$ << Ph–Si(OCH_2CH_2O)$_2$ ≤ F-silicate. Bond length is one of the key factors influencing their reactivity. The present study supported that the C–Si bond length of Ph–Si(OCH_2CH_2O)$_2$ was longer than that of Ph–Si(OMe)$_3$ in organic solvents, which is consistent with its

View Article Online
DOI: 10.1039/D6CP00617F

high reactivity in the Hiyama cross-coupling reaction. Importantly, steric hindrance around the C–Si bonds is also crucial to determine their reactivity in the Hiyama cross-coupling. Ph–Si(OCH_2CH_2O)$_2$ and Ph–Si(OMe)$_3$ adopt square-pyramidal and tetrahedral geometries, which provide sterically less-hindered environments to facilitate the transmetallation step. In contrast, Ph–Si(OMe)$_3$F possesses sterically hindered trigonal bipyramidal geometry, and remains unreactive (Scheme 2), despite having the longest C–Si bond length. This unreactivity is consistent with the findings of Amatore and Jutand.[32]

3. Conclusions

In conclusion, we established a new soft X-ray absorption spectroscopy technique, Soft-XAS-OS, that enables the analysis of sp²-hybridized carbons in organic solvents. The development of this method is the significant progress from Soft-XAS-H_2O, which measured the XAS spectra of organic molecules in aqueous solutions, because most organic reactions are conducted in organic solvents. By measuring the energy thresholds of representative organic solvents and the C=C and C=N π* peak positions of organic molecules, we confirmed that the electronic states of sp²-hybridized carbons can be distinguished from solvent absorbances. Through comparison with inner-shell calculations combined with the MD simulations, Soft-XAS-OS provides insights into the bond lengths in organic solvents, as demonstrated for the investigation of the electronic structures of an arylsilane and silicates with different reactivities in the Hiyama cross-coupling reaction. The solvent effects and the deviations of the liquid structures were included in the present inner-shell calculations, whose calculation schemes would be useful for other spectroscopic techniques such as IR spectroscopy for studying the bond lengths of organic molecules in solutions. The observed XAS spectral shifts are rationalized in terms of C–Si bond elongation, and the reactive glycol-derived silicate Ph–Si(OCH_2CH_2O)$_2$ exhibits longer C–Si bonds compared to the less reactive species Ph–Si(OMe)$_3$. The Soft-XAS-OS, combined with inner-shell calculations, provides a powerful approach for probing electronic structures and offers insights into the bond lengths of organic molecules in organic solvents. This method could be applicable to a variety of bond-forming organic reactions involving sp² carbons, including various cross coupling reactions.

Author contributions

Masanari Nagasaka: conceptualization, data curation, formal analysis, funding acquisition, investigation, methodology, project administration, resources, supervision, validation, visualization, writing-original draft, writing-review & editing; Shintaro Okumura: conceptualization, data curation, formal analysis, funding acquisition, investigation, methodology, project administration, resources, supervision, validation, visualization, writing-original draft, writing-review & editing; Shun Ichii: investigation, data curation, formal analysis, methodology; Go Hamasaka: conceptualization, investigation, data curation, formal analysis, methodology; Yasuhiro Uozumi: conceptualization, data curation, formal analysis, funding acquisition, investigation, methodology, project administration, resources, supervision, validation, visualization, writing-original draft, writing-review & editing.

Conflicts of interest

There are no conflicts to declare.

Data availability

All data supporting the findings of this study are available within supplementary information (SI). Supplementary information: General methods and materials; C K-edge XAS spectra of organic solvents; C K-edge XAS spectra of organic molecules containing sp² carbons; preparations of arylsilanes and silicates; stoichiometric reactions; DFT predicted ^{19}F NMR; inner-shell calculations; and cartesian coordinates. See DOI: 10.1039/x0xx00000x.

Acknowledgements

This work was supported by JSPS KAKENHI grants JP19H02680, JP24K17688 and JP 25K03396, as well as by the Joint Research program of the Institute for Molecular Science (IMS program Nos. 21-101, and 22IMS1102). XAS experiments were performed at the BL3U beamline of the UVSOR Synchrotron Facility, Institute for Molecular Science (IMS program Nos. 21-624 and 22IMS6617). The inner-shell calculations were performed using resources of the Research Center for Computational Science, Okazaki, Japan (Nos. 22-IMS-C187 and 25-IMS-C226, and 26-IMS-C238).

References

1 H. B. Burgi, J. D. Dunitz and E. Shefter, *J. Am. Chem. Soc.*, 1973, **95**, 5065-5067.
2 P. Murray-Rust, H. B. Buergi and J. D. Dunitz, *J. Am. Chem. Soc.*, 1975, **97**, 921-922.
3 P. G. Jones and A. J. Kirby, *J. Chem. Soc., Chem. Commun.*, 1979, 288-289.
4 F. H. Allen and A. J. Kirby, *J. Am. Chem. Soc.*, 1984, **106**, 6197-6200.
5 A. J. Briggs, R. Glenn, P. G. Jones, A. J. Kirby and P. Ramaswamy, *J. Am. Chem. Soc.*, 1984, **106**, 6200-6206.
6 P. G. Jones and A. J. Kirby, *J. Am. Chem. Soc.*, 1984, **106**, 6207-6212.
7 P. G. Jones and A. J. Kirby, *J. Chem. Soc., Chem. Commun.*, 1986, 444-445.
8 V. Ferretti, P. Gilli, V. Bertolasi and G. Gilli, *Crystallogr. Rev.*, 1996, **5**, 3-98.
9 M. Nagasaka, T. Hatsui, H. Setoyama, E. Rühl and N. Kosugi, *J. Electron Spectrosc. Relat. Phenom.*, 2011, **183**, 29-35.

10 S. Bordiga, E. Groppo, G. Agostini, J. A. van Bokhoven and C. Lamberti, *Chem. Rev.*, 2013, **113**, 1736-1850.
11 J. Timoshenko and B. R. Cuenya, *Chem. Rev.*, 2021, **121**, 882-961.
12 C. T. Chantler, *J. Phys. Chem. Ref. Data*, 2000, **29**, 597-1048.
13 J. W. Smith and R. J. Saykally, *Chem. Rev.*, 2017, **117**, 13909-13934.
14 M. Nagasaka, H. Yuzawa and N. Kosugi, *Anal. Sci.*, 2020, **36**, 95-105.
15 M. Nagasaka and N. Kosugi, *Chem. Lett.*, 2021, **50**, 956-964.
16 T. W. Ford, A. D. Stead and R. A. Cotton, *Electron Microsc. Rev.*, 1991, **4**, 269-292.
17 C. Spielmann, N. H. Burnett, S. Sartania, R. Koppitsch, M. Schnürer, C. Kan, M. Lenzner, P. Wobrauschek and F. Krausz, *Science*, 1997, **278**, 661-664.
18 E. J. Takahashi, T. Kanai, K. L. Ishikawa, Y. Nabekawa and K. Midorikawa, *Phys. Rev. Lett.*, 2008, **101**, 253901.
19 M. Nagasaka, K. Mochizuki, V. Leloup and N. Kosugi, *J. Phys. Chem. B*, 2014, **118**, 4388-4396.
20 M. Nagasaka, M. Bouvier, H. Yuzawa and N. Kosugi, *J. Phys. Chem. B*, 2022, **126**, 4948-4955.
21 Y. Yao, M. Nagasaka and K. Mochizuki, *Physica A*, 2024, **647**, 129917.
22 M. Nagasaka, H. Yuzawa and N. Kosugi, *Z. Phys. Chem.*, 2018, **232**, 705-722.
23 S. Tsuru, B. Sharma, M. Nagasaka and C. Hättig, *J. Phys. Chem. A*, 2021, **125**, 7198-7206.
24 M. Nagasaka, H. Yuzawa and N. Kosugi, *J. Phys. Chem. B*, 2020, **124**, 1259-1265.
25 H. Yuzawa, M. Nagasaka and N. Kosugi, *J. Phys. Chem. C*, 2015, **119**, 7738-7745.
26 S. Ichii, G. Hamasaka and Y. Uozumi, *Chem. Asian J.*, 2019, **14**, 3850-3854.
27 T. Hatsui, E. Shigemasa and N. Kosugi, *AIP Conf. Proc.*, 2004, **705**, 921-924.
28 G. Cooper, M. Gordon, D. Tulumello, C. Turci, K. Kaznatcheev and A. P. Hitchcock, *J. Electron Spectrosc. Relat. Phenom.*, 2004, **137-140**, 795-799.
29 M. Nagasaka, H. Yuzawa, K. Mochizuki, E. Rühl and N. Kosugi, *J. Phys. Chem. Lett.*, 2018, **9**, 5827-5832.
30 Y. Nakao and T. Hiyama, *Chem. Soc. Rev.*, 2011, **40**, 4893-4901.
31 T. Komiyama, Y. Minami and T. Hiyama, *ACS Catal.*, 2017, **7**, 631-651.
32 C. Amatore, L. Grimaud, G. Le Duc and A. Jutand, *Angew. Chem. Int. Ed.*, 2014, **53**, 6982-6985.
33 K. H. Shukla and P. DeShong, *J. Org. Chem.*, 2008, **73**, 6283-6291.
34 W. Chen, E. C. X. Ang, S. M. Tan, Z. Chua, J. Ren, Z. Yang, B. Teng, R. Lee, H. Lu and C.-H. Tan, *J. Am. Chem. Soc.*, 2020, **142**, 19065-19070.
35 Note that the widely broad peak at −136.0 ppm would be hypercoordinate complexes, undergoing dynamic processes such as ligand exchange and pseudorotation.
36 F. Frati, M. O. J. Y. Hunault and F. M. F. de Groot, *Chem. Rev.*, 2020, **120**, 4056-4110.
37 M. Nagasaka, H. Yuzawa, T. Horigome and N. Kosugi, *J. Electron Spectrosc. Relat. Phenom.*, 2018, **224**, 93-99.
38 M. J. Abraham, T. Murtola, R. Schulz, S. Páll, J. C. Smith, B. Hess and E. Lindahl, *SoftwareX*, 2015, **1-2**, 19-25.
39 N. A. Murugan, Z. Rinkevicius and H. Ågren, *J. Phys. Chem. A*, 2009, **113**, 4833-4839.
40 W. L. Jorgensen and J. Tirado-Rives, *Proc. Natl. Acad. Sci. U. S. A.*, 2005, **102**, 6665-6670.
41 L. S. Dodda, I. C. de Vaca, J. Tirado-Rives and W. L. Jorgensen, *Nucleic Acids Res.*, 2017, **45**, W331-W336
42 L. S. Dodda, J. Z. Vilseck, J. Tirado-Rives and W. L. Jorgensen, *J. Phys. Chem. B*, 2017, **121**, 3864-3870.
43 N. Kosugi and H. Kuroda, *Chem. Phys. Lett.*, 1980, **74**, 490-493.
44 N. Kosugi, *Theor. Chim. Acta*, 1987, **72**, 149-173.
45 S. Tsuru and M. Nagasaka, *J. Phys. Chem. A*, 2025, **129**, 3020-3031.
46 M. Nagasaka, *J. Chem. Phys.*, 2023, **158**, 024501.

View Article Online DOI: 10.1039/D6CP00617E

View Article Online
DOI: 10.1039/D6CP00617E

Data Availability Statement

All data supporting this article have been included as part of the Supplementary Information.